CrystEngComm

Accepted Manuscript

ROYAL SOCIETY OF CHEMISTRY

www.rsc.org/crystengcomm

Cite this: DOI: 10.1039/c0xx00000x

www.rsc.org/xxxxxx

ARTICLE TYPE

Synthesis of hollow rare-earth compound nanoparticles by a universal sacrificial template method

Yue Jia,[‡a] Tian-Ying Sun,[‡a] Jia-Hong Wang,[a] Hao Huang,[a,c] Penghui Li,[b,c] Xue-Feng Yu,[*a,b,c] Paul K. Chu[*c]

Received (in XXX, XXX) Xth XXXXXXXXX 20XX, Accepted Xth XXXXXXXXX 20XX

DOI: 10.1039/b000000x

A universal technique to synthesize hollow nanoparticles including spindle-like YVO_4, urchin-like YPO_4, and bowl-like $NaYF_4$ by a sacrificial process utilizing the $Y(OH)CO_3$ template is described. X-ray diffraction (XRD), scanning electron microscopy (SEM), transmission electron microscopy (TEM), Fourier transform infrared (FTIR) spectroscopy, and N_2 adsorption-desorption measurements reveal that the hollow nanoparticles with a controllable size are produced due to the Kirkendall phenomenon. Bright fluorescence can be obtained by doping the nanoparticles with lanthanide ions such as Eu^{3+}, Ce^{3+}/Tb^{3+}, and Yb^{3+}/Er^{3+}. These hollow nanoparticles exhibiting bright fluorescence have potential in fluorescence-guided drug-delivery applications and this universal and effective technique can be employed to fabricate various types of hollow materials.

1. Introduction

Synthesis of inorganic hollow materials with controllable composition and shape has aroused much attention due to their superior properties such as low density, large specific surface area, and good permeability.[1,2] These hollow materials with special functional properties such as fluorescence, magnetism, *etc*. have many potential applications including drug delivery,[3,4,5] cell labeling,[6,7] photodynamic therapy,[8,9] sensing,[10,11] catalysis,[12] and waste removal.[13] Up to now, the template process is the most common and efficient method to fabricate these hollow nanostructured materials. Based on templates such as silica,[14-16] carbon spheres,[17] and polystyrene beads,[18,19] hollow nanospheres with the desirable morphology and pure phase have been prepared. However, fabrication and removal of the templates involve multiple steps are time consuming and the templates often introduce environmental energy consumption concerns.[20,21] Recently, sacrificial-template synthesis utilizing the nanoscale Kirkendall effect has been proposed as an efficient method to produce hollow structures because it can avoid the template removal process and simultaneously produce a controllable morphology. Therefore, this approach has aroused increasing interest in the preparation of various types of functional nanomaterials.[20-26]

Rare-earth compounds have unique optical, catalytic, and magnetic properties.[27-31] In particular, rare-earth compounds such as fluorides, phosphates, and vanadates are promising alternatives to organic fluorophores on account of their attractive optical and chemical features such as low toxicity, large Stokes shifts, high resistance to photobleaching, and photochemical degradation, *etc*.[32-34] One area of special interest in the introduction of rare-earth elements into well-defined hollow nanostructures.[11,21,25,35-39] For example, lanthanide-doped $GdVO_4$ hollow spheres possess multifunctionality and can be used in upconversion cell imaging, MRI, and pH-dependent drug release.[25] Hollow GdF_3 spheres with both bright luminescence and drug-release properties have large potential in drug-delivery systems and targeted cancer therapy.[21] However, the synthesis of various types of rare-earth compounds with a hollow structure by a universal method has not been demonstrated.

In this paper, a universal method to synthesize different kinds of hollow rare-earth compound nanoparticles by chemical transformation of the sacrificial template is described. The $Y(OH)CO_3$ template is first prepared by a urea-based homogeneous precipitation method and serves as a sacrificial template to produce YVO_4, YPO_4, and $NaYF_4$ nanoparticles. Different fluorescence properties can be obtained from the nanoparticles by doping with lanthanide ions.

2. Experimental Section

2.1 Materials

$Y(NO_3)_3{\cdot}6H_2O$ (99.99%), $Eu(NO_3)_3{\cdot}6H_2O$ (99.99%), $Yb(NO_3)_3{\cdot}6H_2O$ (99.99%), $Er(NO_3)_3{\cdot}6H_2O$ (99.99%), NH_4VO_3 (99%), $NH_4H_2PO_4$ (99%), $NaBF_4$ (99.99%), polyethyleneimine (PEI) (MW = 10,000), and urea were purchased from Sigma-Aldrich and other reagents were obtained from Sinopharm Chemical Reagent Co. Ltd. All the reagents were used as received without further purification and ultrapure water was used throughout the experiments.

2.2 Preparation of $Y(OH)CO_3$:Ln^{3+} Spheres

The monodispersed $Y(OH)CO_3$:Ln^{3+} (Ln = Eu, Yb/Er, Ce/Tb) spherical particles were prepared *via* a urea-based homogeneous precipitation process according to the literature with some

modifications.[35] $RE(NO_3)_3{\cdot}6H_2O$ (RE = Y, Eu, Yb, Er, Ce, and Tb) was dissolved in ultrapure water at a concentration of 0.5 mol L^{-1}. In a typical procedure to synthesize Ln-doped (Ln = Eu, Yb/Er, Ce/Tb) yttrium hydroxycarbonate [$Y(OH)CO_3$:5%Eu^{3+}, Eu/(Eu + Y) molar ratio = 5%; $Y(OH)CO_3$: 20%Yb^{3+}, 3%Er^{3+}, Yb/(Yb + Er + Y) molar ratio = 20%, Er/(Yb + Er + Y) molar ratio = 3%; $Y(OH)CO_3$: 20%Ce^{3+}, 20%Tb^{3+}, Ce/(Ce + Tb + Y) molar ratio = 20%, Tb/(Ce + Tb + Y) molar ratio = 20%] and using $Y(OH)CO_3$:Eu^{3+} as an example, 2 mL of $Y(NO_3)_3{\cdot}6H_2O$, 0.105 mL of $Eu(NO_3)_3{\cdot}6H_2O$, and 1.5g of urea [$CO(NH_2)_2$] were dissolved in ultrapure water. The total volume of the solution was 100 mL. The solution was homogenized by magnetic stirring at room temperature for 30 min and reacted at 95 °C for 3 h in an oil bath. The products were purified by centrifugation at 6,000 rpm for 5 min and washed with ethanol and water thrice.

2.3 Preparation of YVO_4:Ln^{3+}, YPO_4:Ln^{3+} Hollow Spheres

In a typical experiment, the as-prepared $Y(OH)CO_3$:Eu^{3+} precipitate was dispersed in 30 mL of water and sonicated for 30 min to obtain a uniform solution. 0.176 g of NH_4VO_3 (V/Y molar ratio = 1.5) was added to the solution and after additional agitation for half an hour (pH = 5), the solution was transferred to a Teflon bottle (50 mL in capacity) in a stainless steel autoclave, sealed, and maintained at 180 °C for 12 h. The YPO_4:Ce^{3+}, Tb^{3+} (P/Y molar ratio = 1.5) was prepared by the same procedures as YVO_4:Eu^{3+}, except using $Y(OH)CO_3$:Ce^{3+}, Tb^{3+} and $NH_4H_2PO_4$ as starting materials. Before the solution was transferred to the autoclave, the pH value was about 5.0. The suspension was separated by centrifugation at 6,000 rpm for 5 min after it was cooled to room temperature by a hydro-cooling process. Finally, the products were collected, washed with ultrapure water and ethanol thrice, and dried overnight at 50 °C in a vacuum oven. The pH values of the final YVO_4:Eu^{3+} and YPO_4:Ce^{3+}, Tb^{3+} products were about 5.0.

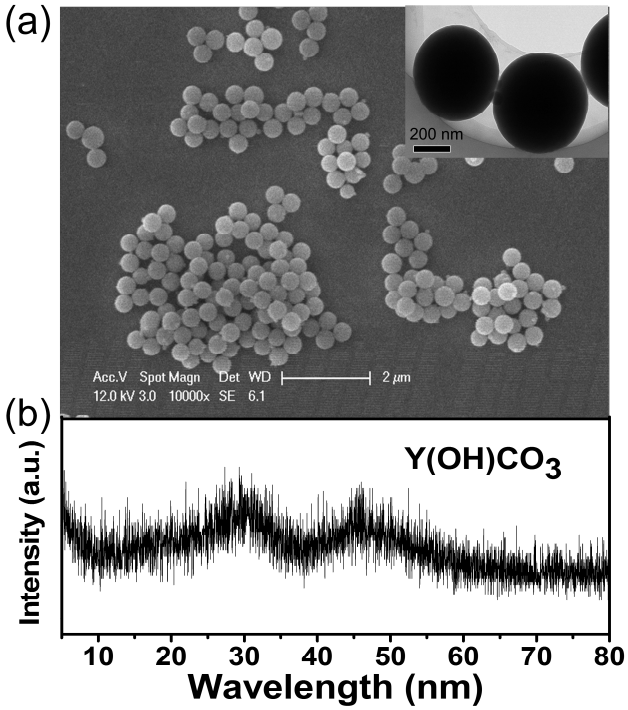

Fig. 1 (a) SEM with inset TEM image and (b) XRD patterns of the $Y(OH)CO_3$ precursors.

2.4 Preparation of $NaYF_4$:Ln^{3+} Hollow Spheres

In a typical experiment to prepare the $NaYF_4$:Ln^{3+} spheres, the as-prepared $Y(OH)CO_3$:Yb^{3+}, Er^{3+} sample, and 1 g of PEI were dispersed in 20 mL of ultrapure water by ultrasonification for 30 min to obtain solution. 4 mmol of $NaBF_4$ was added to the solution and after additional agitation for 10 min (pH = 9), the solution was transferred to a Teflon bottle (50 mL in capacity) in a stainless steel autoclave, sealed, and maintained at 180 °C for 3.5 h. The resulting suspension was separated by centrifugation at 6,000 rpm for 5 min after it was cooled to the room temperature by a hydro-cooling process. Finally, the products were collected, washed with ultrapure water and ethanol thrice, and dried overnight at 50 °C in a vacuum oven. The pH value of the final $NaYF_4$: Yb^{3+}, Er^{3+} product was about 5.0.

2.5 Characterization

X-ray diffraction (XRD) was performed on a Bruker D8-advance X-ray diffractometer with Cu $K_{\alpha 1}$ irradiation (λ = 1.5406 Å). The sample morphology and structure were investigated by scanning electron microscopy (FE-SEM, Siron, FEI) and transmission electron microscopy (TEM, JEM 2010 HT). The excitation and emission spectra were recorded on a Hitachi F-4500 fluorescence spectrophotometer equipped with a Xenon lamp as the excitation source. The Fourier transform infrared (FTIR) spectra were acquired on a NICOLET 5700 FTIR spectrometer. N_2 adsorption-desorption studies were undertaken using an ASAP 2020 Micromeritics Instrument at 77 K. The samples were degassed at 120 °C overnight in vacuum. The optical excitation source in the upconversion measurements was a Ti: sapphire laser system (Mira 900-F).

3. Results and Discussion

The $Y(OH)CO_3$ precursors doped with Ln^{3+} ions were synthesized by a general urea-based homogenous precipitation method[40] and their composition and phase purity are shown in Fig. 1. The precursor shows no obvious diffraction peak but two broad bands at 30° and 48° suggesting that the precursor is amorphous. Although there is no unit cell and crystal symmetry information in JCPDS file for this structure, the component can be inferred to be $Y(OH)CO_3$ according to previous literature.[41] As shown in the SEM and TEM images in Fig. 1, the $Y(OH)CO_3$ particles manifest as uniform and solid spheres with a mean diameter of 400 nm and the surface of the solid spheres is smooth. These as-prepared $Y(OH)CO_3$ spheres serve as the precursor of subsequent reactions.

The YVO_4:Ln^{3+} (Ln = Eu) spheres are synthesized by the reaction between $Y(OH)CO_3$:Ln^{3+} precursors and NH_4VO_3 under hydrothermal conditions at 180 °C for 12 h and the morphology and crystal structure are shown in Fig. 2. The YVO_4:Ln^{3+} (Ln = Eu) spheres have a spindle-like morphology with average minor and major axis lengths of 180 nm and 340 nm. The enlarged TEM image indicates that the individual spindle-like particles are composed of many tiny packed YVO_4 grains with different

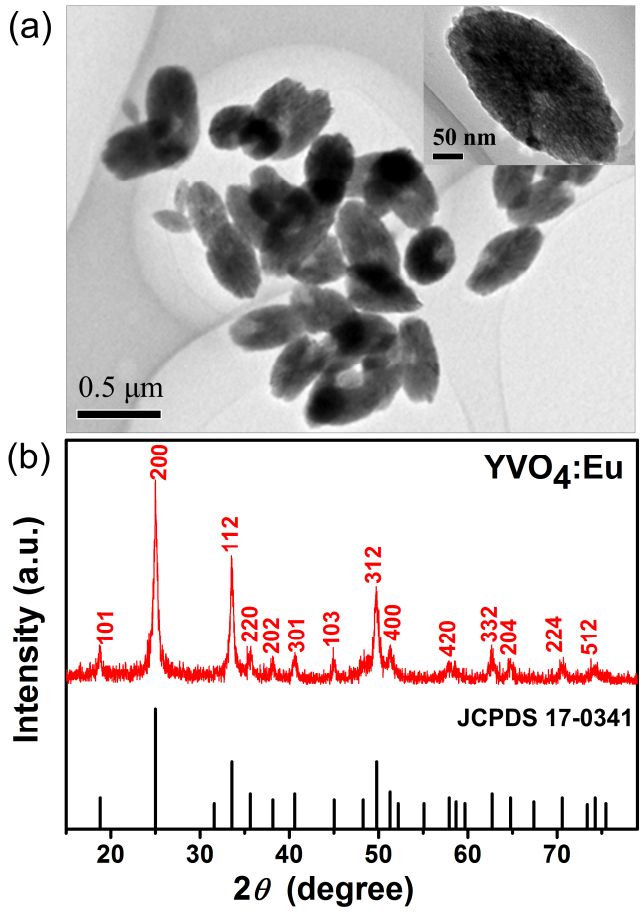

Fig. 2 (a) TEM images and (b) XRD patterns of the $YVO_4:Eu^{3+}$ particles.

orientations which can be confirmed by N_2 adsorption-desorption. As shown in the XRD pattern, all the peaks are in good agreement with the standard JCPDS card 17-0341 of YVO_4. The structure of the nanoparticles is tetragonal in nature. The size of the crystalline domains obtained from the X-ray line broadening by using Scherrer equation is about 17 nm. In the Scherrer equation, $D = 0.89\lambda / \beta\cos\theta$, where D is the crystal size in nanometers, λ stands for the x-ray wavelength (0.15406 nm), β is the angular line width at half maximum (FWHM) intensity, and θ denotes the diffraction angle of the observed peak. The intense diffraction (200) peak is selected to calculate the crystallite size. It should be noted that this is the approximate size of the spindle-like particles since the Scherrer equation is more suitable for the calculation of spherical particles.

The $YPO_4:Ln^{3+}$ particles can also be synthesized by using the similar method used to prepare the $YVO_4:Ln^{3+}$ particles with $Y(OH)CO_3$ being the precursor (see Fig. 3). Under hydrothermal conditions (180 °C for 12 h), the $YPO_4:Ce^{3+}$, Tb^{3+} spheres are synthesized by the reaction between the $Y(OH)CO_3$ precursors and $NH_4H_2PO_4$. The XRD patterns in Fig. 3b can be indexed to the YPO_4 phase, indicating a tetragonal phase with a body-centered structure of YPO_4 (JCPDS card 42-0082). The crystallite size of the Ce^{3+}, Tb^{3+} co-doped YPO_4 estimated from the intense diffraction peak of (200) is 32 nm. Fig. 3a shows the SEM and TEM images of the $YPO_4:Ce^{3+}$, Tb^{3+} particles. Nearly monodispersed and uniform spheres with a mean diameter of around 260 nm are shown in Fig. 3a. Compared to the $Y(OH)CO_3$ precursor, the surface of the spheres is rough and covered by nanothorns consisting of aggregates of numerous small nanorods. It should be noted that the diameter of the spheres becomes smaller with respect to the sacrificial template (Fig. 1). To clearly reveal the structure of the urchin-like YPO_4 spheres, TEM is performed. The inset in Fig. 3a depicts a typical TEM image of the stacked nanorod building blocks and it is in agreement with the SEM image of the urchin-like YPO_4 spheres. Owing to the relatively high transmission ability of electron beam at the center than the margin, the interior hollow structure of the spheres can be inferred.

By employing the aforementioned method, $NaYF_4:Ln^{3+}$ particles can also be synthesized using $Y(OH)CO_3$ as the precursors (see Fig. 4). Under hydrothermal conditions of 180 °C for 3.5 h, the $NaYF_4:Ln^{3+}$ (Ln = Yb/Er) spheres are synthesized by the sacrificial process of $Y(OH)CO_3$. As shown in Fig. 4b, all the diffraction peaks of the products can be indexed to the pure cubic phase structure of $NaYF_4$ (JCPDS 77-2042). No obvious reflection from $Y(OH)CO_3$ can be found suggesting complete transformation. The size and morphology of the product are studied by SEM and the particles have a homogenous size distribution and good dispersion characteristic of the $Y(OH)CO_3$ template. Each sphere is slightly larger (about 480 nm in diameter) than the template and has a rather rough surface. The

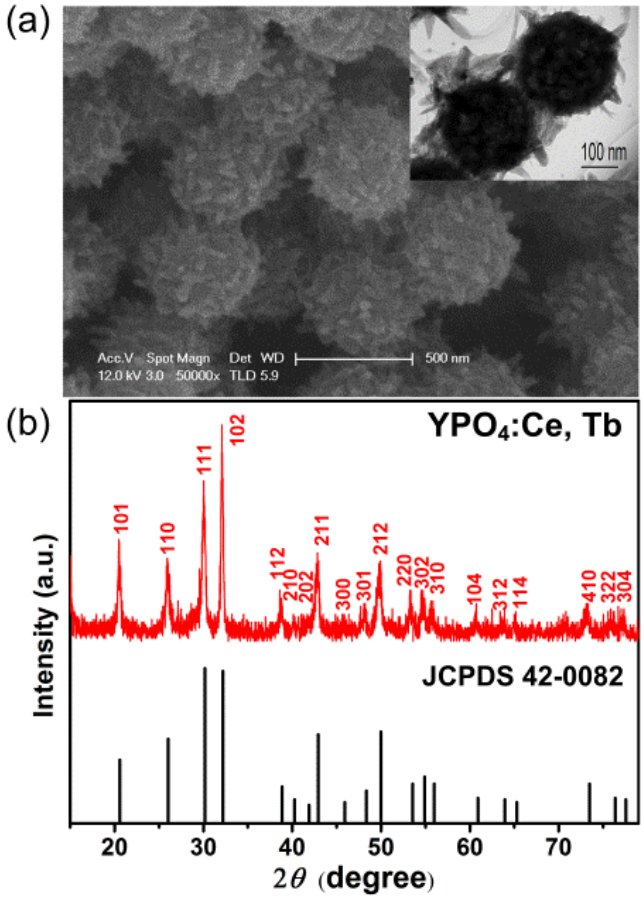

Fig. 3 SEM (a) with inset TEM image and (b) XRD patterns of the $YPO_4:Ce^{3+}$, Tb^{3+} particles.

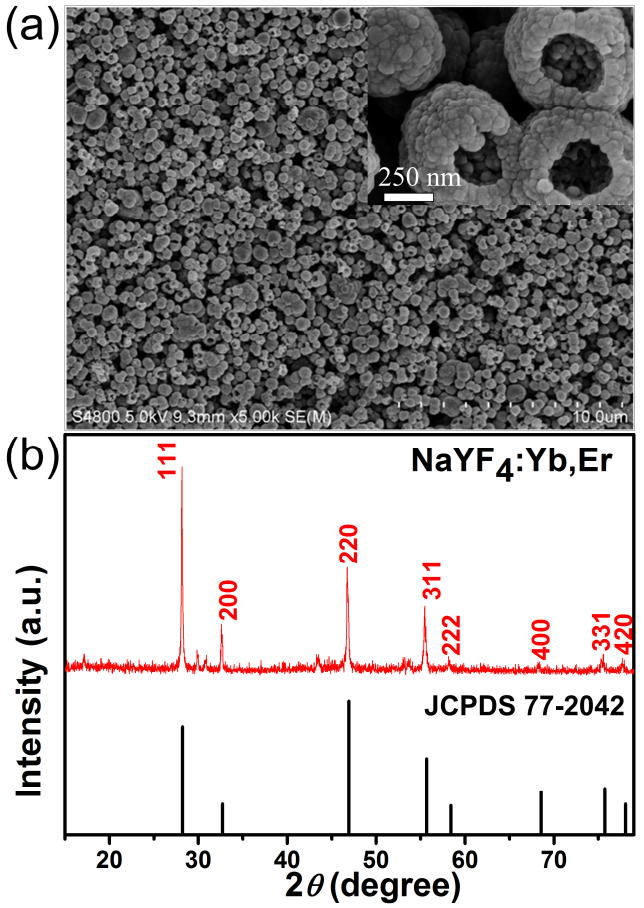

Fig. 4 (a) SEM images and (b) XRD patterns of the $NaYF_4$:Yb^{3+}, Er^{3+} particles.

interior cavity can be clearly observed from the broken spheres. Furthermore, each bowl-like particle is composed of numerous interconnected irregular shaped nanoparticles. These stacked crystalline building blocks are randomly assembled but distributed homogeneously throughout the large particle. The abundant interior space among the building blocks yields the hollow structures.

The above results demonstrate a universal sacrificial template method to synthesize various types of hollow rare-earth compound nanoparticles, as illustrated in Scheme 1. Firstly, the

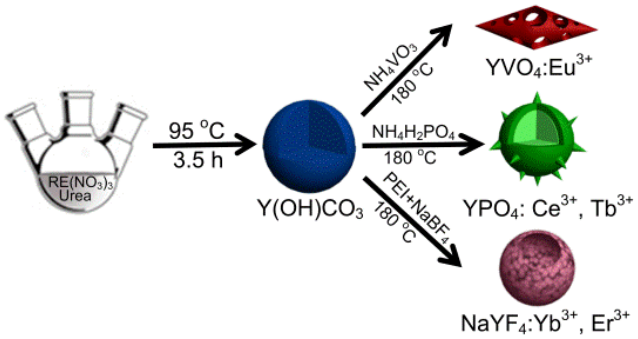

Scheme 1 Schematic illustration of the preparation of spindle-like YVO_4:Eu^{3+}, urchin-like YPO_4:Ce^{3+}, Tb^{3+}, and bowl-like $NaYF_4$:Yb^{3+}, Er^{3+} particles.

$Y(OH)CO_3$ spheres are synthesized *via* a homogenous precipitation progress. The $Y(OH)CO_3$ spheres are employed as both the physical and chemical template in the following hydrothermal process. Formation of the hollow spheres is based on a fundamental solid-state phenomenon, the Kirkendall effect, which deals with different diffusion rates between diffusion couples.[1,39,42-44] With regard to the formation of the YVO_4 hollow structures, the diffusion couples are Y^{3+} ions inside and the VO_4^{3-} ions outside. The detailed reaction processes are listed below:

$$(VO_3)_n^{n-} + nH_2O \rightarrow nVO_4^{3-} + 2nH^+ \quad (1)$$
$$3H^+ + Y(OH)CO_3 \rightarrow Y^{3+} + 2H_2O + CO_2 \quad (2)$$
$$Y^{3+} + VO_4^{3-} \rightarrow YVO_4 \quad (3)$$

In the initial stage at a high temperature and pressure, H^+ and VO_4^{3-} are released according to reaction (1). Subsequently, as shown by reaction (2), H^+ corrodes the $Y(OH)CO_3$ spheres producing a large amount of Y^{3+} most of which is located on the $Y(OH)CO_3$ spheres. Y^{3+} reacts with VO_4^{3-} under the solution followed by the quick formation of a thin YVO_4 layer at the solid-liquid interface according to equation (3). The YVO_4 layer prevents the direct chemical reaction and further reaction relies on diffusion of Y^{3+} and VO_4^{3-}. Finally, fast outward diffusion of Y^{3+} and slow inward diffusion of VO_4^{3-} through the YVO_4 layer (Kirkendall effect) lead to faster production of YVO_4 on the external surface of the YVO_4 layer than the internal one. As a result, continuous consumption of the $Y(OH)CO_3$ spheres and lower growth rate on the internal surface of the YVO_4 layer are responsible for the formation of YVO_4 hollow spheres.

A similar Kirkendall phenomenon can be found from the preparation of hollow YPO_4 and $NaYF_4$.

For YPO_4:

$$NH_4H_2PO_4 \rightarrow NH_4^+ + PO_4^{3-} + 2H^+ \quad (1)$$
$$3H^+ + Y(OH)CO_3 \rightarrow Y^{3+} + 2H_2O + CO_2 \quad (2)$$
$$Y^{3+} + PO_4^{3-} \rightarrow YPO_4 \quad (3)$$

For $NaYF_4$:

$$BF_4^- + 3H_2O \rightarrow BO_3^{3-} + 6H^+ + 4F^- \quad (1)$$
$$3H^+ + Y(OH)CO_3 \rightarrow Y^{3+} + 2H_2O + CO_2 \quad (2)$$
$$Na^+ + Y^{3+} + 4F^- \rightarrow NaYF_4 \quad (3)$$

It should be noted that the dominant phosphate and borate species in the synthesis processes may be slightly different from those mentioned in the above chemical equations because of the dependence on the reaction pH. However, these intermediate products have little impact on the final products of YPO_4 or $NaYF_4$.

In the formation of YPO_4, more Y^{3+} diffuses outwards to the YPO_4 layer decreasing the $Y(OH)CO_3$ spheres resulting in emergence of the initial voids and filament-like bridges (inset TEM image in Fig. 3) which may provide faster transportation paths for outward delivery of Y^{3+}.[45] The larger diffusion rate of Y^{3+} of the phosphate phase can be ascribed to a lower crystallinity in comparison to the vanadate solid.

The formation mechanism for $NaYF_4$ is also attributed to the Kirkendall effect and very similar to YVO_4 discussed above. The diffusion couples for the Kirkendall effect are Y^{3+} from the inside and F^- ions from the outside. H^+ and F^- are first released from BF_4^- due to equation (1) and then H^+ corrodes the $Y(OH)CO_3$ template to create Y^{3+} that is located on the surface of the $Y(OH)CO_3$ spheres (equation (2)). In the meantime, F^- and Na^+ diffuse gradually near the $Y(OH)CO_3$ sphere and react with Y^{3+}

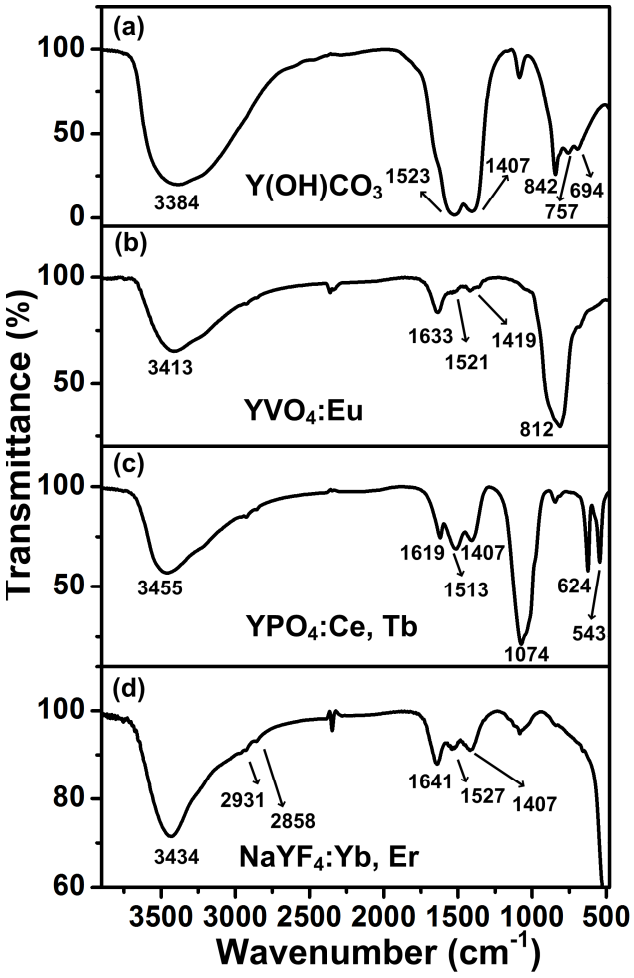

Fig. 5 FTIR spectra of (a) $Y(OH)CO_3$, (b) $YVO_4:Eu^{3+}$, (c) $YPO_4:Ce^{3+}$, Tb^{3+}, and (d) $NaYF_4$: Yb^{3+}, Er^{3+} particles.

around the precursor template to form the initial $NaYF_4$ layer (equation (3)). Since outward diffusion of Y^{3+} is faster than that inward of F^-, $NaYF_4$ gradually gathers on the outside of the initial $NaYF_4$ layer. As the template $Y(OH)CO_3$ is consumed, the large central hole gradually appears. PEI provides a favorable chemical environment for the formation of soluble and stable $NaYF_4$ during the hydrothermal process. Besides, the polymer chains of PEI possess abundant amine groups including about 25% primary amines, 50% of secondary amines, and 25% of tertiary amines, thereby rendering a platform for direct surface functionalization with biomolecules through bioconjugate chemistry.[34,46]

In order to further understand the composition and surface structure of the particles, FTIR is conducted on the precursors and final products. As shown in Fig. 5a, the characteristic absorption bands of O-H (3384 cm^{-1}), symmetric O-C-O (1523 cm^{-1} and 1407 cm^{-1}), π-CO_3^{2-} (842 cm^{-1}), and δCO_3^{2-} (757 cm^{-1} and 694 cm^{-1}) can be observed demonstrating the presence of the carbonate group. Comparing to curve a, the characteristic adsorption peaks of CO_3^{2-} in curves b, c, and d decrease significantly (1521 cm^{-1} and 1419 cm^{-1} for YVO_4, 1513 cm^{-1} and 1407 cm^{-1} for YPO_4, as well as 1527 cm^{-1} and 1407 cm^{-1} for $NaYF_4$), indicating that the composition of the hydrothermal products have changed. For YVO_4, besides the decrease of the carbonate group, the intensity transmittance peak at 812 cm^{-1} is the characteristic vibration of the V-O bond in the VO_4^{3-} group.

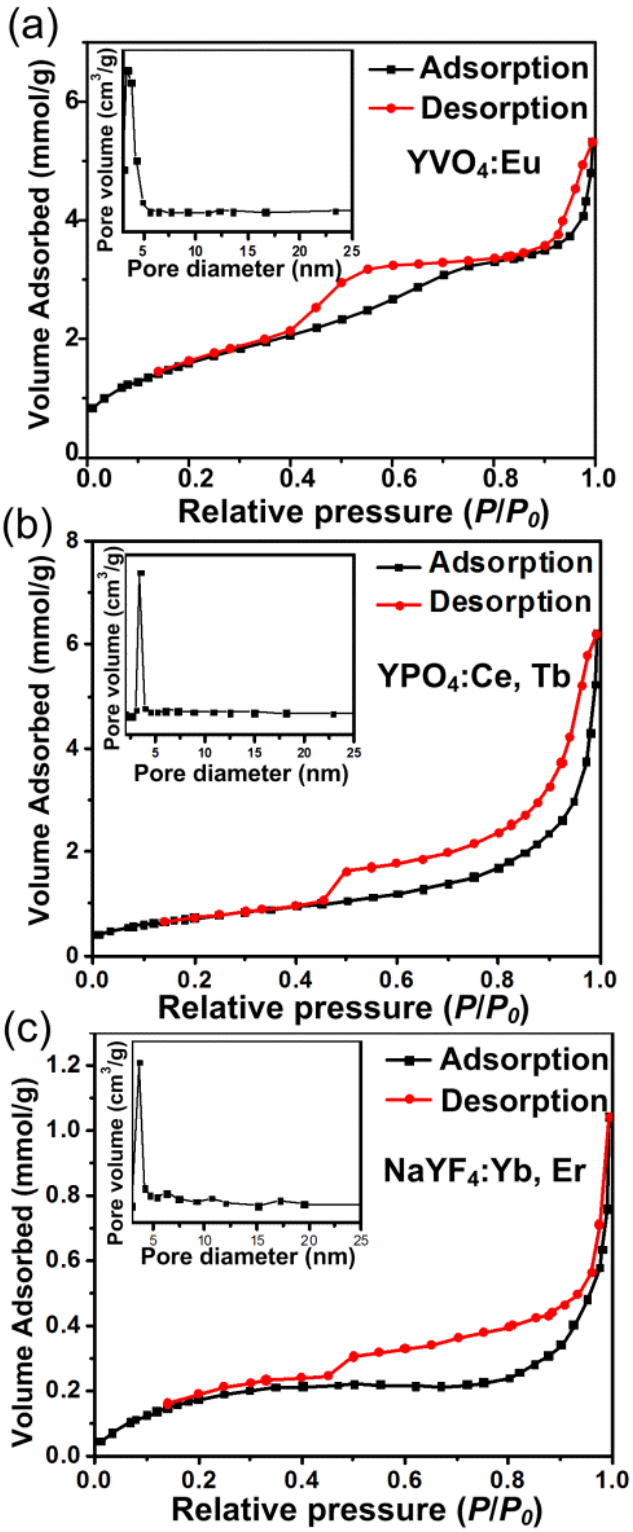

Fig. 6 N_2 adsorption-desorption isotherms and pore size distribution curves: (a) Hollow $YVO_4:Eu^{3+}$, (b) Hollow $YPO_4:Ce^{3+}$, Tb^{3+}, and (c) Hollow $NaYF_4:Yb^{3+}$, Er^{3+} particles.

Furthermore, some bands at 3413 cm^{-1} and 1633 cm^{-1} can be observed and are attributed to the stretching and bending vibrations of O-H, implying that the surface of the YVO_4 particles contain O-H groups and H_2O.

For YPO_4, the characteristic absorption peaks at 1074 cm^{-1} and at 543 cm^{-1}, 624 cm^{-1} are due to the stretching and bending vibration within PO_4^{3-} groups. In addition, it can be seen a weaker absorption at 1619 cm^{-1} and a very broad feature at about 3455 cm^{-1}, attributed to the stretching and bending of the O-H vibration.

For $NaYF_4$ particles, the existence of PEI adsorbed on the surface can be proved by the FTIR results. The effect of PEI is demonstrated by the presence of absorption bands from the internal vibration of the amide bonds (1641 cm^{-1}) and -CH_2 stretching vibrations (2858 cm^{-1} - 2931 cm^{-1}). The 2858 cm^{-1} and 2931 cm^{-1} bands are, respectively, the symmetric and asymmetric stretching vibrations. The characteristic O-H vibrations are also observed at 3434 cm^{-1}, originating from the absorption of H_2O.

The N_2 adsorption-desorption isotherms and pore size distributions in Fig. 6 provide further evidence for the formation of pores in the large primary YVO_4:Ln^{3+}, YPO_4:Ln^{3+}, and $NaYF_4$:Ln^{3+} particles. These hollow structures show the type IV isotherm and typical H1 hysteresis loop typical of mesoporous materials.[47] The BET specific surface area is a measure of a solid object and compares the surface area of the object relative to mass. The BET surface area of these samples are 132, 59.3, and 16.7 m^2g^{-1} and the pore volume is 0.19, 0.22, and 0.04 cm^3g^{-1}, respectively. The pore size distributions derived from the desorption branch using the Barrett–Joyner–Halenda (BJH) method (inset in Fig. 6) show narrow apexes at 3.4, 3.5, and 3.7 nm, respectively. The peak of the pore size distribution curve only represents the most probable value of the pore size. The results indicate that the reaction between $Y(OH)CO_3$ as a sacrificial template and VO_3^-, PO_4^{3-}, Na^+, and F^- as starting materials is an effective approach to prepare hollow materials with a controllable size and shape.

The photoluminescence properties of the hollow rare-earth compound nanoparticles are displayed in Fig. 7. The excitaiton spectrum (Fig. 7a, left) of YVO_4: Eu^{3+} consists of a strong absorption band with a maximum at 294 nm (monitoring at 615 nm) which can be assigned to the energy transfer from the oxygen ligand (O^{2-}) to central vanadium ion (V^{5+}) inside VO_4^{3-}.[48] The emisson spectrum (Fig. 7a, right) shows four groups of emission lines at about 594, 615, 648, and 697 nm, which are ascribed to the electric dipole transition of Eu^{3+} from the $^5D_0$ level to sublevel of ^7F_J (J = 1, 2, 3, 4), respectively, whereas the weak peak at 538 nm can be attributed to the transition of $^5D_1$-$^7F_1$. No emission from the VO_4^{3-} groups can be detected, revealing that the energy transfer from VO_4^{3-} to Eu^{3+} is very efficient. The $^5D_0$-$^7F_2$ (615 nm) transition of Eu^{3+} is dominant representing an electric-dipole allowed transition and hypersensitive to the environment. The strong red emission of the sample can be seen clearly from the inset in Fig. 7a. In contrast, no emission can be observed from the precursor of $Y(OH)CO_3$:Eu^{3+} due to the low crystallinity of the host.

The excitation and emission spectra of the YPO_4:Ce^{3+}, Tb^{3+} particles are depicted in Fig. 7b. By monitoring the emission of Tb^{3+} at 548 nm, the allowed f-d transitions of Ce^{3+} can be observed whereas the forbidden f-f transitions of Tb^{3+} are almost nonexistent, implying efficient electron transfer from Ce^{3+} to Tb^{3+}. Under 280 nm excitation, the characteristic emission of Tb^{3+} for

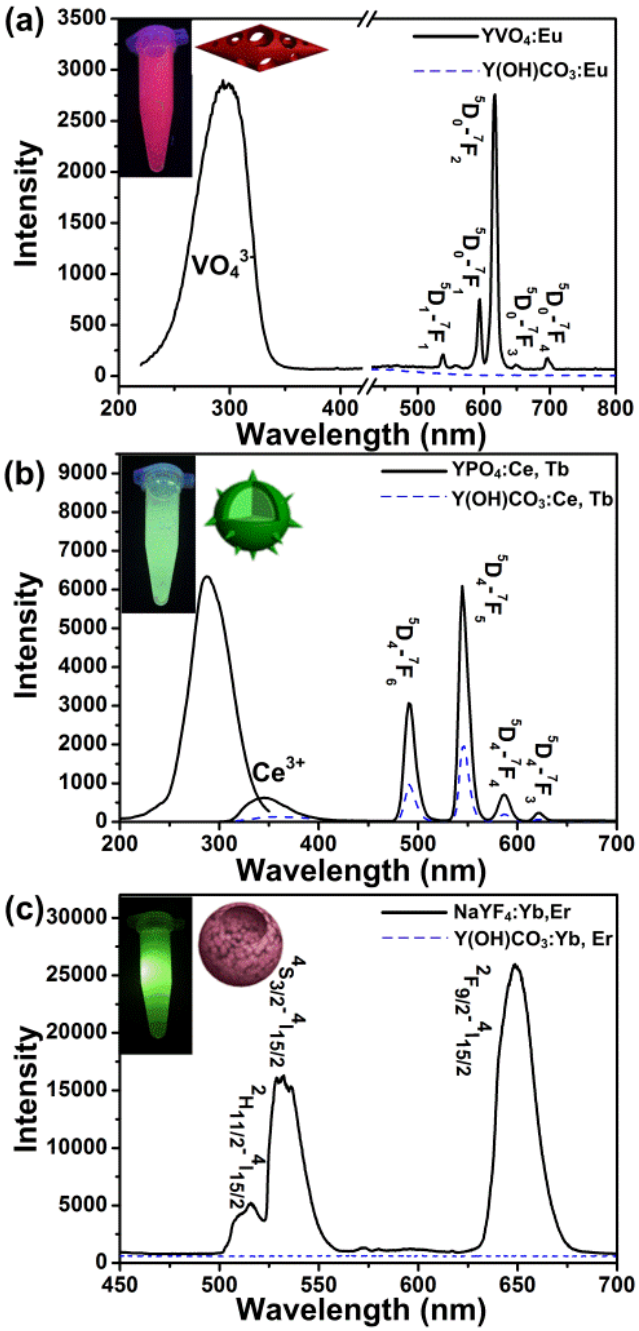

Fig. 7 (a) Excitation spectra (λ_{em} = 615 nm, left) of YVO_4:Eu^{3+} particles, and emission spectra (λ_{ex} = 294 nm, right) of YVO_4:Eu^{3+} and $Y(OH)CO_3$:Eu^{3+} particles. (b) Excitation spectra (λ_{em} = 548 nm, left) of YPO_4:Ce^{3+}, Tb^{3+} particles, and emission spectra (λ_{ex} = 294 nm, right) of YPO_4:Ce^{3+}, Tb^{3+} and $Y(OH)CO_3$: Ce^{3+}, Tb^{3+} particles. (c) Emission (λ_{ex} = 294 nm) spectra of $NaYF_4$: Yb^{3+}, Er^{3+} and $Y(OH)CO_3$: Yb^{3+}, Er^{3+} particles. The inset images are the corresponding morphological model and the photographs taken from the samples under 254 nm (a-b) or 980 nm light (c) irradiation.

the $^5D_4$-^7F_J (J = 6, 5, 4, 3) transitions ranges from 494 nm to 623 nm together with the UV Ce^{3+} emission at 350 nm. In general, direct excitation of Tb^{3+} is difficult and inefficient due to the Laporte forbidden f-f transition.[49] The electronic transitions for the $4f^n$ configurations of Tb^{3+} are forbidden so that they nearly disappear from the absorption spectrum. However, excitation that produces a high light output can be achieved by exciting a different ion (a sensitizer, *i.e.*, Ce^{3+}). Herein, by taking advantage of the allowed electronic transition, Ce^{3+} acts as the sensitizer which transfers the excitation energy to Tb^{3+} and so the energy-transfer process from Ce^{3+} to Tb^{3+} can enhance Tb^{3+} emission thus giving rise to bright and efficient Tb^{3+} green emission. It can also be oberseved that the emission intensity of YPO_4:Ce^{3+}, Tb^{3+} is three times that of the $Y(OH)CO_3$:Ce^{3+}, Tb^{3+} particles.

$NaYF_4$ has been found to be the most efficient host lattice for upconversion luminescence of lanthanide ions that can sequential absorb two or more photons leading to the emission of the output radiation at a shorter wavelength than the excitation wavelength.[50,51] Here, Yb^{3+} and Er^{3+} are incorporated into the hollow $NaYF_4$ particles to investigate their upconversion properties (see Fig. 7c). The optimal wavelenghth for pumping light to attain upconversion is 980 nm, which matches the $^2F_{7/2}$-$^2F_{5/2}$ transition of Yb^{3+}. The emission bands are assigned to transitions of the 4f-4f levels of Er^{3+}. The transitions from $^2H_{11/2}$ and $^4S_{3/2}$ to the Er^{3+} ground state $^4I_{15/2}$ yield bright green emissions at 515 nm and 532 nm, respectively and their emission band at 648 nm is assigned to the Er^{3+} electronic transition $^4F_{9/2}$-$^4I_{15/2}$.[52] Due to the same reason mentioned above, no upconversion emission can be oberved in the precursor of $Y(OH)CO_3$:Yb^{3+}, Er^{3+} particles.

Conclusion

A universal hydrothermal sacrificial-template method to synthesize different kinds of hollow nanostructured particles is described. The $Y(OH)CO_3$ spheres are used as a sacrificial template which acts as the precursor and controls the morphology. SEM, TEM, FTIR and N_2 adsorption-desorption reveal the hollow structure and the formation mechanism is related to the Kirkendall effect which deals with different diffusion rates of the species. The hollow nanoparticles possess desirable luminescence properties by doping with rare-earth elements. These hollow nanoparticles exhibiting bright fluorescence have large potential in fluorescence-guided drug-delivery applications and the sacrificial template approach is a universal one extendable the preparation of other types of hollow nanostructures.

Acknowledgments

The authors acknowledge the financial support from the Natural Science Foundation of China (NSFC) No. 51372175, Hong Kong Research Grants Council (RGC) General Research Funds (GRF) CityU 112212, and Guangdong - Hong Kong Technology Cooperation Funding Scheme (TCFS) GHP/015/12SZ.

Notes and references

[a] *Department of Physics, Key Laboratory of Artificial Micro- and Nano-structures of Ministry of Education,Wuhan University, Wuhan, P. R. China. E-mail: yxf@whu.edu.cn (X.-F. Yu)*
[b] *Institute of Biomedicine and Biotechnology, Shenzhen Institutes of Advanced Technology, Chinese Academy of Sciences*
[c] *Department of Physics and Materials Science, City University of Hong Kong, Tat Chee Avenue, Kowloon, Hong Kong. E-mail: paul.chu@cityu.edu.hk (P. K. Chu)*
‡ *Yue Jia and Tian-Ying Sun contributed equally to this work.*

1. Y. Yin, R. M. Rioux, C. K. Erdonmez, S. Hughes, G. A. Somorjai and A. P. Alivisatos, *Science*, 2004, **304**, 711.
2. X. Lou, L. A. Archer and Z. Yang, *Adv. Mater.*, 2008, **20**, 3987.
3. Z. Xu, Y. Cao, C. Li, P. Ma, X. Zhai, S. Huang, X. Kang, M. Shang, D. Yang, Y. Dai and J. Lin, *J. Mater. Chem.*, 2011, **21**, 3686.
4. Z. Xu, P. Ma, C. Li, Z. Hou, X. Zhai, S. Huang and J. Lin, *Biomaterials*, 2011, **32**, 4161.
5. D. Yang, X. Kang, P. Ma, Y. Dai, Z. Hou, Z. Cheng, C. Li and J. Lin, *Biomaterials*, 2013, **34**, 1601.
6. Z. Wang, J. Hao, H. L. W. Chan, W. T. Wong and K. L. Wong, *Small*, 2012, **8**, 1863.
7. G. Wang, Q. Peng and Y. Li, *Accounts of chemical research*, 2011, **44**, 322.
8. Y. Chen, Q. Yin, X. Ji, S. Zhang, H. Chen, Y. Zheng, Y. Sun, H, Qu, Z. Wang, Y. Li, X. Wang, K. Zhang, L. Zhang and J. Shi, *Biomaterials*, 2012, **33**, 7126.
9. L. J. De. Cock, S. De. Koker, B. G. De. Geest, J. Grooten, C. Verveat, J. P. Remon, G. B. Sukhorukov and M. N. Antipina, *Angew. Chem. Int. Ed.*, 2010, **49**, 6954.
10. H. J. Kim, K. I. Choi, A. Pan, I. D. Kim, H. R. Kim, K. M. Kim, C. W. Na, G. Cao and J. H. Lee, *J. Mater. Chem.*, 2011, **21**, 6549.
11. T. Sun, D. Zhang, X. Yu, Y. Xiang, M. Luo, J. Wang, G. Tan, Q. Wang and P. K. Chu, *Nanoscale*, 2013, **5**, 1629.
12. H. Chen, R. S. Liu, M. Y. Lo, S. C. Chang, L. D. Tsai, Y. M. Peng and J. F. Lee, *J. Phys. Chem. C,* 2008, **112**, 7522.
13. Y. Wang, G. Wang, H. Wang, C. Liang, W. Cai and L. Zhang, *Chem. Eur. J.*, 2010, **16**, 3497.
14. P. Yang, S. Gai and J. Lin, *Chem. Soc. Rev.*, 2012, **41**, 3679.
15. Z. Feng, Y. Li, D. Niu, L. Li, W. Zhao, H. Chen, L. Li, J. Gao, M. Ruan and J. Shi, *Chem. Commun*., 2008, **23**, 2629.
16. Y. S. Lin and C. L. Haynes, *Chem. Mater.*, 2009, **21**, 3979.
17. G. Tian, Z. Gu, X. Liu, L. Zhou, W. Yin, L. Yan, S. Jin, W. Ren, G. Xing, S. Li and Y. Zhao, *J. Phys. Chem. C*, 2011, **115**, 23790.
18. X. Cheng, M. Chen, L.Wu and G. Gu, *Langmuir*, 2006, **22**, 3858.
19. Z. Jin, F. Wang, F. Wang, J. Wang, J. Yu and J. Wang, *Adv. Funct. Mater.*, 2013, **23**, 2137.
20. X. Qu, G. Pan, H. Yang, Y. Chen, J. Chung, B. Moon, B. Choi, J. Jeong and K. Jang, *RSC Advance*, 2013, **3**, 4763.
21. R. Lv, S. Gai, Y. Dai, N. Niu, F. He and P. Yang, *ACS Appl. Mater. Interfaces*, 2013, **5**, 10806.
22. F. Zhang, G. B. Braun, Y. Shi, Y. Zhang, X. Sun, N. O. Reich, D. Zhao and G. Stucky, *J. Am. Chem. Soc.*, 2010, **132**, 2850.
23. G. Cheng, J. L. Zhang, Y. L. Liu, D. H. Sun and J. Z. Ni, *Chem. Eur. J.*, 2012, **18**, 2014.
24. Z. Wang, G. Cheng, Y. Liu, J. Zhang, D. Sun and J. Ni, *Small,* 2012, **8**, 3456.
25. H. Ren, L. Zhang, T. Wang, L. Li, Z. Su and C. Wang, *Chem. Commun.*, 2013, **49**, 6036.
26. J. Zhao, X. Liu, D. Cui, Y. Sun, Y. Yu, Y. Yang, C. Du, Y. Wang, K. Song, K. Liu, S. Lu, X. Kong and H. Zhang, *Eur. J. Inorg. Chem.*, 2010, 1813.
27. M. C. Herffern, L. M. Matosziuk and T. J. Meade, *Chem. Rev.*, 2013, DOI: 10.1021/cr400477t.
28. P. A. Tanner, *Chem. Soc. Rev.*, 2013, **42**, 5090.
29. S. Zeng, Z. Yi, W. Lu, C. Qian, H. Wang, L. Rao, T. Zeng, H. Liu, H. Liu, B. Fei and J. Hao, *Adv. Funct. Mater.*, 2014, DOI: 10.1002/adfm.201304270.
30. S. Zeng, M. Tsang, C. Chan, K. Wong and J. Hao, *Biomaterials*, 2012, **33**, 9232.
31. S. Zeng, J. Xiao, Q. Yang and J. Hao, *J. Mater. Chem.*, 2012, **22**, 9870.

32. Y. Liu, D. Tu, H. Zhu and X. Chen, *Chem. Soc. Rev.,* 2013, **42**, 6924.
33. C. Liu, Z. Gao, J. Zeng, Y. Hou, F. Fang, Y. Li, R. Qiao, L. Shen, H. Lei, W. Yang and M. Gao, *ACS Nano*, 2013, **7**, 7227.
34. X. Yu, Z. Sun, M. Li, Y. Xiang, Q. Wang, F. Tang, Y. Wu, Z. Cao and W. Li, *Biomaterials*, 2010, **31**, 8724.
35. D. Zhang, T. Sun, X. Yu, Y. Jia, M. Chen, J. Wang, H. Huang and P. K. Chu, *Materials Research Bulletin*, 2014, **52**, 122.
36. X. Yang, L. Xu, Z. Zhai, F. Cheng. Z. Yan, X. Feng, J. Zhu and W. Hou, *Langmuir*, 2013, **29**, 15992.
37. F. Zhang, G. B. Braun, A. Pallaoro, Y. Zhang, Y. Shi, D. Cui, M. Moskovits, D. Zhao and G. D. Stucky, *Nano Lett.*, 2012, **12**, 61.
38. R. Lv, S. Gai, Y. Dai, F. He, N. Niu and P. Yang, *Inorg. Chem.*, 2014, **53**, 998.
39. L. Zhang, M. Yin, H. You, M. Yang, Y. Song and Y. Huang, *Inorg. Chem.*, 2011, **50**, 10608.
40. S. Lechevallier, P. Lecante, R. Mauricot, H. Dexpert, J. Dexpert-Ghys, H. K. Kong, G. L. Law and K. L. Wong, *Chem. Mater.*, 2010, **22**, 6153.
41. J. Li, X. Li, X. Sun and T. Ishigaki, *J. Phys. Chem. C*, 2008, **112**, 11707.
42. C. Lv, W. Di, Z. Liu, K. Zheng and W. Qin, *Dalton Transactions*, 2014, **43**, 3681.
43. F. Zhang, Y. Shi, X. Sun, D. Zhao and G. D. Stucky, *Chem. Mater.*, 2009, **21**, 5237.
44. J. Zhang, Y. Wang, Z. Xu, H. Zhang, P. Dong, L. Guo, F. Li, S. Xin and W. Zeng, *J. Mater. Chem. B*, 2013, **1**, 330.
45. Y. Yin, C. K. Erdonmez, A. Cabot, S. Hughes and A. P. Alivisatos, *Adv. Funct. Mater.*, 2006, **16**, 1389.
46. X. Yu, M. Li, M. Xie, L. Chen, Y. Li and Q. Wang, *Nano Res*, 2010, **3**, 51.
47. K. S. W. Sing, *Pure & Appl. Chem*., 1982, **54**, 2201.
48. G. Jia, C. Zhang, S. Ding, L. Wang, L. Li and H. You, *CrystEngComm*, 2012, **14**, 573.
49. J. R. Lakowicz, Principles of Fluorescence Spectroscopy, Springer, Singapore, 2006.
50. K. W. Krämer, D. Biner, G. Frei, H. U. Güdel, M. P. Hehlen and S. R. Lüthi, *Chem. Mater.*, 2004, **16**, 1244.
51. F. Wang, Y. Han, C. Lim, Y. Lu, J. Wang, J. Xu, H. Chen, C. Zhang, M. Hong and X. Liu, *Nature*, 2010, **463**, 1061.
52. M. Ding, C. Lu, L. Cao, Y. Ni and Z. Xu, *CrystEngComm*, 2013, **15,** 8366.

Graphical Abstract

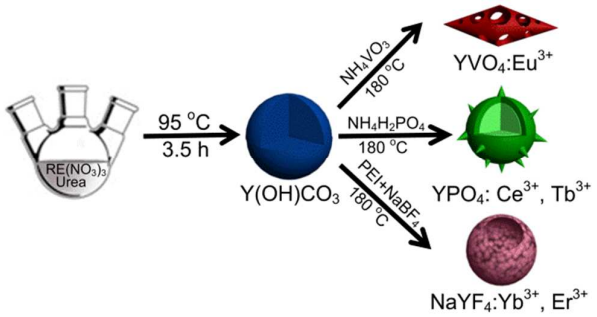

Universal sacrificed-template method to synthesize hollow structured materials with fluorescence properties.